RSC Advances

PAPER

View Article Online
View Journal | View Issue

Cite this: *RSC Adv.*, 2021, **11**, 10827

Mechanically strong polyimide aerogels cross-linked with low-cost polymers

Zhongxin Zhang, [a] Yuelei Pan, *[a] Lunlun Gong,*[a] Xiandong Yao,[b] Xudong Cheng [a] and Yurui Deng [a]

Received 19th December 2020
Accepted 4th March 2021

DOI: 10.1039/d0ra10633j

rsc.li/rsc-advances

Polyimide aerogels were prepared using low-cost polymers with different structure capped polyamide oligomers serving as cross-linking agents. To investigate the effects of the anhydride density on cross-linker chain units and side groups of cross-linkers on their properties and microstructures, two kinds of polymers from maleic anhydride, endic anhydride, and styrene were prepared by simple radical polymerization. The polyimide aerogels exhibit densities as low as 0.087 g cm^{-3} and specific surface areas as high as 456 m^2 g^{-1}. And the maximum modulus of the aerogel is up to 21.3 MPa. These cross-linkers are alternatives to expensive small molecule cross-linkers, therefore reducing the cost of PI aerogels.

Introduction

Aerogels are extremely porous materials with interconnected three-dimensional (3D) network structures.[1–3] Because of the large number of pores filled with air, aerogels exhibit many unique properties, such as high porosity, ultralow density, low thermal conductivity, and large specific surface area.[4–6] However, most of the investigated silica aerogels tend to be fragile because of the pearl necklace structure.[3]

On the other hand, organic aerogels prepared by the sol–gel process from polymer have been attracting much attention from researchers over the past few decades, due to superior mechanical properties, such as polyurea, polystyrene,[7] polyvinyl alcohol,[8] polyacrylonitrile,[9] and polybenzoxazine.[10] However, their thermal properties are poor making them unable to be used in hot environments due to their chemical structure. In this case, it is necessary to improve the thermal stability of aerogels.

Unlike silica aerogels and conventional organic aerogels, polyimide aerogel has excellent mechanical properties (flexibility and pressure resistance),[11,12] good flame retardant properties[13] and thermal decomposition temperature (T_d).[14,15] The excellent mechanical properties and thermal stability are mainly due to the highly rigid aromatic structure and conjugation effects of aromatic ring structures of the imide chain.[16–18] In general, polyimide aerogels are firstly dehydrated at room temperature by chemically aromatic diamides and aromatic diamines in polar solvents (such as *N*,*N*-dimethyl-formamide (DMF), *N*,*N*-dimethylacetamide (DMAc) and *N*-methyl-2-pyrrolidone (NMP)) to form polyamide acid (PAA).[19,20] Polyimide aerogels formed by chemical or thermal imidization reaction, followed by supercritical drying CO_2. Polyimide aerogels obtained by direct chemical or thermal imidization reaction have a linear structure, and therefore the pore structure is susceptible to heat shrinkage, which increases density and thermal conductivity.[21] To improve the shrinkage defect of polyimide aerogels, cross-linked polyimide aerogels were developed. Guo *et al.*[21] used octa-(aminophenyl)-silsesquioxane (OAPS) as the cross-linking agent, 3,3′,4,4′-biphenyl tetracarboxylic dianhydride (BPDA) as dianhydride, bisaniline-*p*-xylidene (BAX) as the diamine, the reaction could occur at room temperature to form aerogels monoliths and thin films, which showed enhancements in thermal and mechanical properties of polyimide aerogels.

The key for preparing cross-linked aerogel is the cross-linkers. At present, the cross-linkers of polyimide are mainly organic small molecules including OAPS, TAB, BTC.[2,22–24] The preparation of these molecules is complex and tedious, and the raw materials are expensive.[25] Furthermore, most of them are harmful to humans and the environment. So the candidates with multiple amino or carboxyl properties have attracted the attention of researchers. Zu *et al.*[26] prepared the polyimide-polyvinylpolymethylsiloxane (PVPMS) composite aerogels cross-linked with amino-modified PVPMS by two different methods: stepwise chemical liquid deposition (SCLD) and direct chemical liquid deposition (DCLD). The aerogels exhibit great mechanical strength. Yan and his team members[27] reported the PI aerogels with excellent mechanical properties. The tensile strength of PI aerogel cross-linked with an ODA-modified multiwalled carbon nanotube reached 141.48 MPa.

Based on the above issues, in this study, we've synthesized two cheap high-performance cross-linkers by a simple method. Furthermore, the effect of the two agents with different side groups and anhydride densities on cross-linker chain units on

[a]*State Key Laboratory of Fire Science, University of Science and Technology of China, Hefei, Anhui 230027, PR China*
[b]*NANO TECH Co., Ltd, Shaoxing, Zhejiang 312366, P. R. China*

aerogel properties were fully investigated. The lowest density of aerogels is as low as 0.087 g cm^{-3} and the maximum surface area is up to 456 m^2 g^{-1}.

Materials and method

Materials

BPDA, ODA, DMBZ, and azobisisobutyronitrile (AIBN) were purchased from Aladdin Chemical Reagent Co. (China). *N*-methyl-2-pyrrolidinone (NMP), anhydrous acetic anhydride, acetone, pyridine, maleic anhydride, styrene, 2-butanone, and toluene were purchased from Sinopharm Chemical Reagent Co. Ltd (China). Endic anhydride (NA) was from Chengdu Kelong Chemical Reagent Co. All reagents were used without further purification.

Synthesis of styrene-maleic anhydride copolymer (PSMA) (Fig. 1a)

A flask with three necks was charged with azobisisobutyronitrile (AIBN) (33 mg, 0.2 mmol), maleic anhydride (9.806 g, 100 mmol), styrene (St) (10.415 g, 100 mmol), 30 mL 2-butanone, and 150 toluene and stirred under nitrogen atmosphere. After stirred for 20 min, the mixture was heated to 60 °C for 24 h. After removing the solvent by filtration, the white power was washed with toluene three times. The toluene was removed under vacuum at 60 °C. This gave 19.8 g (89.2% yield) of PSMA.

Synthesis of endic anhydride maleic anhydride copolymer (PMN) (Fig. 1a)

A flask with three necks was charged with azobisisobutyronitrile (AIBN) (33 mg, 0.2 mmol), maleic anhydride (9.806, 100 mmol), endic anhydride (NA) (16.416 g, 100 mmol), 30 mL 2-butanone, and 150 mL toluene and stirred under nitrogen atmosphere. After stirred for 20 min, the mixture was heated to 60 °C for 24 h. After removing the solvent by filtration, the white power was washed with toluene three times. The toluene was removed under vacuum at 60 °C. This gave 25.6 g (97.7% yield) of PMN.

Preparation of polyimide aerogels

The preparation process of polyimide aerogels is showed in Fig. 1b. Polyamide acid oligomer with the repeat units n of 20, 30, 40 obtained by using the ratio of dianhydride BPDA (n) to diamine ODA and DMBZ ($n + 1$) was synthesized in NMP. As an example, the preparation of the 5% PI aerogels with PSMA cross-linked and $n = 30$. ODA (9.3 mmol, 1.88 g) was dissolved in 55 mL of NMP under magnetic stirring. Then, BPDA (8.4 mmol, 2.648 g) was added. The mixture was stirred for 30 min at room temperature to form an oligomer. Subsequently, PSMA (121 mg) was added with stirring until a homogeneous solution was obtained. After which acetic anhydride (74.4 mmol, 7.26 mL, 8 : 1 M ratio to ODA) and pyridine (74.4 mmol, 7.26 mL, 1 : 1 M ratio to acetic anhydride) were added into the solution. Afterward, the solution was poured into the polypropylene mould and gelled. Then the gels were aged for 24 h in the mould at room temperature. After which, the wet gels were sequentially immersed in 75%, 25% NMP solution in acetone, and 100% acetone for 24 h for solvent exchange. Finally, the monolithic PI aerogels were obtained using supercritical fluid CO_2 drying (55 °C, 12 MPa, 48 h), followed by vacuum drying for 12 h at 60 °C to remove any residual acetone.

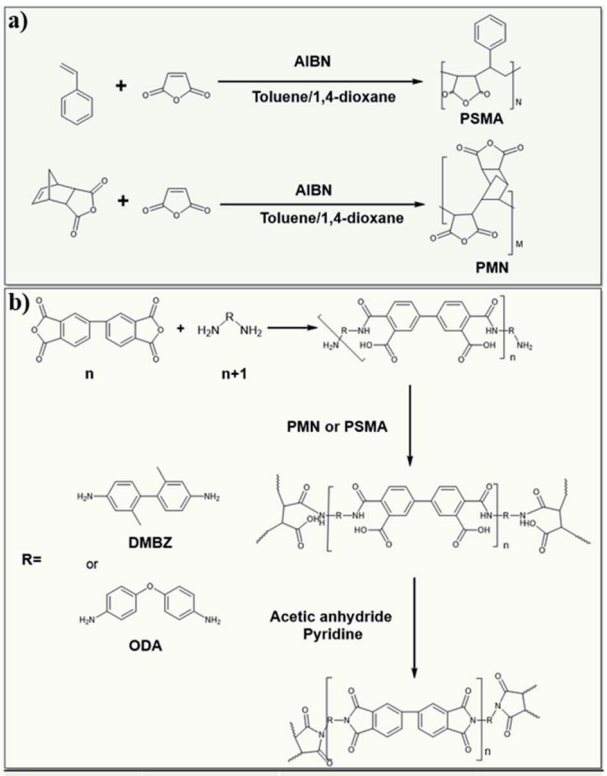

c)

Cross-linkers	Structure	Source	Cost (USD/g)
TAB		Alfa, China	113
OAPS		Macklin, China	168
PSMA		This work	0.18
PMN		This work	0.20

Fig. 1 (a) Synthetic routes for PMN and PSMA; (b) synthetic routes for polyimide aerogels; (c) comparison of commercial cross-linkers and this work's crosslinkers.

Characterization

The bulk density, ρ_b, was calculated by dividing the weight of the sample by the volume. The shrinkage was calculated from the volume difference between the gel sample and the polypropylene mould. The porosity (Π) was calculated based on the bulk and skeletal densities as shown in eqn (1)

$$\prod = \left(1 - \frac{\rho_b}{\rho_s}\right) \times 100\% \quad (1)$$

The specific surface areas and total pore volume of pores were measured by nitrogen sorption isotherms with standard

Brunauer–Emmett–Teller (BET) analysis (Tristar II 3020M, Micromeritics Instrument Corporation, USA). The pore size distributions (PSD) were estimated by the Barrett–Joyner–Halenda (BJH) method (Tristar II 3020M, Micromeritics Instrument Corporation, USA). All samples were degassed at 80 °C for 24 h under vacuum before analysis. Fourier transform infrared spectra (FT-IR, Nicolet 8700, Thermo Fisher Scientific, USA) were obtained to investigate the chemical bonding state of these aerogel samples. Solid ^{13}C NMR spectra of the polymers were obtained on a Bruker AVANCE AV III 400WB spectrometer using the 89 mm solids probe with magic angle spinning at 15 kHz and cross-polarization. Spectra were externally referenced to the carbonyl peak of glycine (176.1 ppm relative to TMS). A Hitachi S-8220 field emission microscope was used for the scanning electron microscope (SEM) images after 60 seconds of sputter coating the specimens with platinization. Thermal gravimetric analyses (TGA) were performed using a TA model SDT Q600 instrument. Samples were run at a temperature ramp rate of 10 °C min^{-1} from room temperature to 800 °C under nitrogen. Uniaxial compression test was performed using an electronic dynamic and static fatigue testing machine (E3000K8953, Instron) with a constant loading rate of 1 mm min^{-1}. The specimens were cut and polished to make sure that the top and bottom surfaces were smooth and parallel. Samples were conditioned at room temperature for 48 h before testing. The diameter and length of the specimens were measured before testing. The Young's modulus was taken as the initial linear portion of the slope of the stress–strain curve.

Results and discussion

The different cross-linkers with different side group densities were prepared by co-polymerizing styrene or endic anhydride with maleic anhydride according to Fig. 1a to investigate the effect of cross-linkers. It is worth noting that these cross-linkers obtained by simple free radical polymerization are less costly than small-molecule cross-linkers, such as TAB, which is costs hundreds of times more than the polymers (Fig. 1c). Polyimide aerogels with two kinds of diamine, using different cross-linkers and polymer concentration from 5 to 10% were prepared to assess the effect of these variables. Fig. 2a shows the preparation process of polyimide aerogels. The aerogels conform to the shape of the moulds and exhibit excellent blocks.

The morphology of the PI aerogels

SEM images of representative aerogels in the study made with 5 wt% polymer concentration are shown in Fig. 2c and d. Unlike polyimide aerogels reported in the literature,[28] the aerogel fibers cross-linked with PMN and PSMA exhibit a flat ribbon structure. This is likely due to the compatibility between the cross-linkers and polyimide chains. Unlike small-molecule cross-linkers, the main chains of cross-linkers are the aliphatic structure, which tends to cluster themselves around each other. The interaction of cross-linkers and the polyimides results in the aerogel forming the ribbon-like fiber structure illustrated in Fig. 2b. It is noticed that at the same polymer concentration, the aerogels cross-linked with PMN have wider and thicker fibers than the

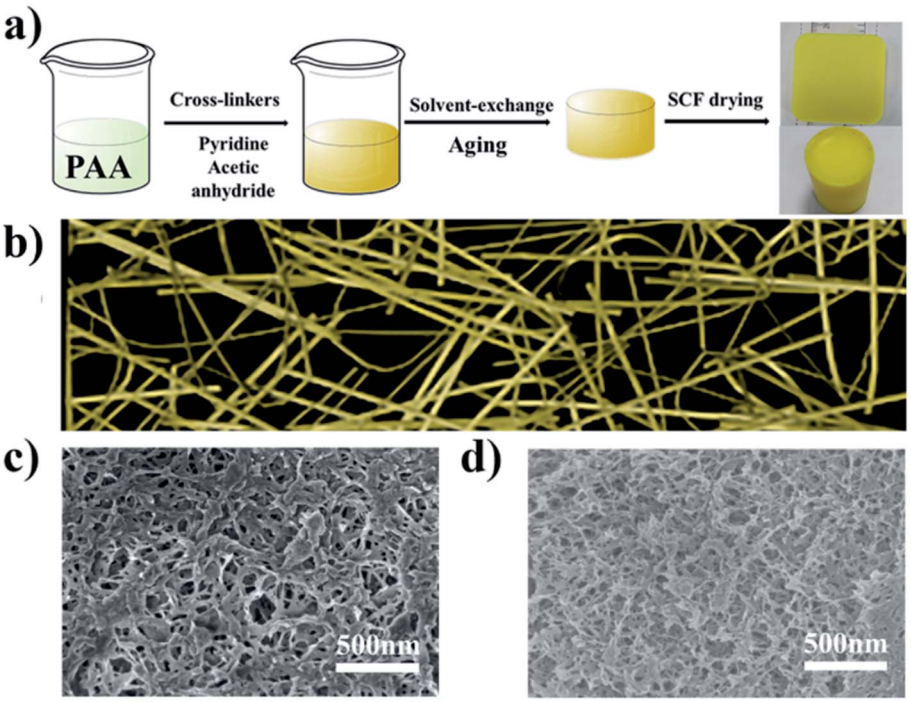

Fig. 2 (a)The preparation process of polyimide aerogels; (b) diagram of polyimide aerogel fiber model; (c) SEM image of PMN-ODA-5; (d) SEM image of PSMA-ODA-5.

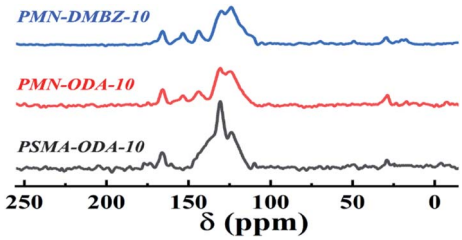

Fig. 3 Solid ^{13}C NMR spectra of polyimide aerogels: PMN-DMBZ-10, PMN-ODA-10 and PSMA-ODA-10.

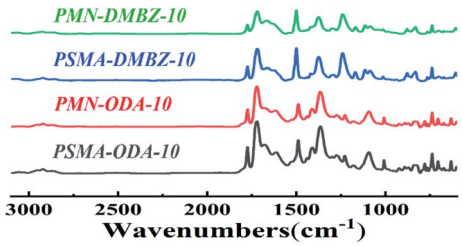

Fig. 4 FT-IR spectra of polyimide aerogels: PMN-DMBZ-10, PSMA-DMBZ-10, PMN-ODA-10, PSMA-ODA-10.

aerogels cross-linked with PSMA. The two cross-linker polymers chains may have different anhydride densities and side groups, leading to their different conformations in solvent NMP. The differences in fiber structure were formed due to the degree of stretching of the cross-linker polymer chains affecting the further stacking of polyimide chains when they reacted with polyamide-acid oligomers. The movement of PSMA molecular chains in solvents is more restricted, leading to a narrower and thinner fibrous band. Due to the poor compatibility of the two polymers with the highly polar solvent NMP, the cross-linker solution and the polyamide acid oligomer solution reacted and cross-linked with each other before they could be dispersed, resulting in the formation of ribbons instead of cylindrical fibers.

The chemical structure of the PI aerogels

Solid ^{13}C NMR spectra of the polyimide aerogels, as seen in Fig. 3, of all spectra contain an imide carbonyl peak at 166 ppm as well as broad aromatic peaks between 108 and 140 ppm characteristic of these polyimides. The aerogels made with ODA show a peak at 153 ppm characteristic of the aromatic ether carbon. The aerogels made with DMBZ give an aliphatic peak at 19 ppm for the pendant methyl groups. The aerogels made using PMN as the cross-linkers show a wider aliphatic peak at 19 ppm than the aerogels made using PSMA as the cross-linkers because of more aliphatic chains of PMN.

Fourier transform infrared (FT-IR) spectra of the samples shows absorption peaks at 1370 cm^{-1}, 1721 cm^{-1}, and 1775 cm^{-1} for C–N stretching band, C=O asymmetric stretching band, and C=O symmetric stretching band of imide, respectively (Fig. 4). As no peak is noticed for the anhydride stretching band at 1860 cm^{-1}, it is assumed that anhydride has been consumed. Peaks disappear at 1660 cm^{-1} and 1535 cm^{-1} for the amide C=O stretching band and amide C–N respectively, indicating that the imidization reaction is complete. The bands at 1807 cm^{-1} and 980 cm^{-1} are absent, ruling out the presence of polyimide isomers. The bands at 720 cm^{-1}, 1440 cm^{-1}, 2858 cm^{-1}, and 2925 cm^{-1} for C–H wagging band, out of plane bending band, symmetric stretching band, and asymmetric stretching band, respectively, are contributed to the aliphatic chains of cross-linkers PMN and PSMA.

The porosity of polyimide aerogels made from different polymer concentrations (wt%) from 5% to 10% with two different cross-linkers and two kinds of diamines are listed in Table 1. Both cross-linkers with different structures were discussed to probe the effect of reaction sites on the structural units. The polymer concentration was investigated since the polymer concentration has a great influence on the shrinkage and porosity of aerogels.[23] The molar ratios of diamine and dianhydride are 31 : 30 on mixing to exclude the influence of the repeat unit number n on aerogel shape.

Table 1 Properties of the different polyamide aerogels investigated in this study

Sample	Cross-linkers	Diamine	Polymer concentration (wt%)	Bulk density (g cm^{-3})	Shrinkage (wt%)	Porosity (%)	Surface area (m^2 g^{-1})	Modulus (MPa)
PMN-DMBZ-5	PMN	DMBZ	5	0.087 ± 0.004	14.7 ± 0.3	93.8 ± 5.3	456	4.4 ± 0.2
PMN-ODA-5	PMN	ODA	5	0.098 ± 0.005	15.2 ± 0.4	92.8 ± 5.1	353	2.9 ± 0.2
PMN-DMBZ-7.5	PMN	DMBZ	7.5	0.117 ± 0.005	9.6 ± 0.3	91.7 ± 5.0	414	8.5 ± 0.6
PMN-ODA-7.5	PMN	ODA	7.5	0.121 ± 0.005	10.3 ± 0.3	91.1 ± 5.1	316	6.8 ± 0.5
PMN-DMBZ-10	PMN	DMBZ	10	0.136 ± 0.005	6.7 ± 0.2	90.3 ± 4.3	364	21.3 ± 0.9
PMN-ODA-10	PMN	ODA	10	0.145 ± 0.005	7.6 ± 0.3	89.6 ± 4.1	258	13.6 ± 0.8
PSMA-DMBZ-5	PSMA	DMBZ	5	0.093 ± 0.004	14.9 ± 0.5	93.4 ± 5.2	429	2.8 ± 0.2
PSMA-ODA-5	PSMA	ODA	5	0.108 ± 0.005	15.7 ± 0.4	92.1 ± 5.1	332	1.6 ± 0.2
PSMA-DMBZ-7.5	PSMA	DMBZ	7.5	0.124 ± 0.005	10.5 ± 0.4	91.2 ± 4.8	385	7.4 ± 0.5
PSMA-ODA-7.5	PSMA	ODA	7.5	0.135 ± 0.005	12.4 ± 0.3	90.5 ± 4.6	296	6.9 ± 0.5
PSMA-DMBZ-10	PSMA	DMBZ	10	0.151 ± 0.005	7.3 ± 0.3	89.2 ± 4.4	327	16.8 ± 0.8
PSMA-ODA-10	PSMA	ODA	10	0.174 ± 0.005	7.9 ± 0.3	88.7 ± 4.3	231	11.6 ± 0.6

The shrinkage of the PI aerogels

The shrinkage of aerogels occurs during the fabrication of gels, solvent exchange, and supercritical CO_2 drying.[2] As with all polyimide aerogels, polymer concentration plays an important role in the contraction process. As expected, the shrinkage of the aerogel decreases as the polymer concentration increases (Fig. 5a). The aerogels with DMBZ as diamines exhibit a smaller shrinkage (Fig. 5d and Table 1). This is contributed to the synergy of solvent effect, chain rigidity, and accumulation.[23] As expected, the aerogels using PMN show less shrinkage and bulk density relative to the aerogels using PSMA from the same concentrated solution and diamide according to Fig. 5a and d. It is most likely due to the differences in polymer chain structure and conformation of cross-linkers because of solvent effect, chain flexibility, and density of reaction units. The cross-linkers show different conformations in NMP due to the different side groups and the density of the anhydride, leading to the difference in cross-linking aerogels molecular rigidity. Fig. 6 shows three-dimensional rendering models of both polymer cross-linkers using MM2. The oligomers are shown with different colors representing atoms residing. It's worth noting that the red oxygen atoms of PSMA are propelled by isometric spirals around the polymer's helical molecular chains while the oxygen atoms of PMNs are randomly distributed on random line clusters of molecular chains. This means that the movement of PSMA molecular chains in solvents is more restricted, leading to a relatively low stacking of their cross-linked polymers so that the shrinkage of aerogels is lower. Similar to aerogels cross-linked with other small molecules, ODA-prepared aerogels show a greater degree of shrinkage due to the relaxation effect of oxygen atoms in the molecule resulting in a greater π–π stack of polyimide oligomers.[29–31] It is worth noting that the shrinkage of aerogels cross-linked with PSMA and PMN is much lower than that of aerogels cross-linked with TAB,[2] OAPS,[22] BTC[28] at the same polymer concentration and diamine.

The porous properties of the PI aerogels

It is expected that the increase in polymer concentration results in increased density and decreased shrinkage of aerogels, which in turn leads to a decrease in porosity (Fig. 5a and b). This is since polymer concentration has a greater effect on it than shrinkage. The density and porosity of aerogels are influenced by the shrinkage when the polymer concentration is constant according to Fig. 5a and b. The crosslinker has a negligible effect on porosity (Fig. 5b) but shows an opposite trend to the effect of shrinkage (Fig. 5c and d). With DMBZ as the diamine, the *F* of the ANOVA was 0.177 and the Sig was 0.695 for different cross-linking agents and polymer concentrations, while with ODA as the diamine, the *F*-value of the ANOVA was 0.243 and the Sig was 0.209 for different cross-linking agents and solid contents. It was proved that the porosity of the aerogels had little correlation with the cross-linking agents. And the maximum porosity of aerogels is up to 93.4% and the minimum density is as low as 0.087 g cm^{-3} (sample PMN-DMBZ-5), which is lower than the density of the PI aerogel cross-linked TAB,[2] OAPS,[22] BTC.[28]

Based on the Brunauer–Emmett–Teller (BET) method, the N_2 adsorption–desorption isotherms of aerogels with both cross-linkers. The isotherms of aerogels cross-linked with both polymers exhibit IUPAC type IV curves with an H1 hysteresis loop

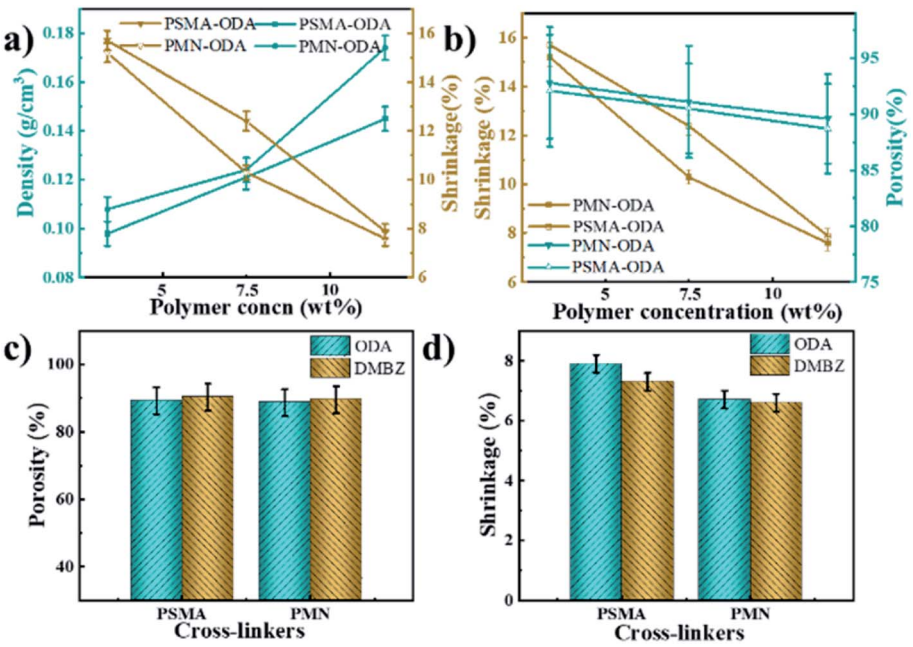

Fig. 5 (a) Density and shrinkage of aerogels prepared with different crosslinkers at different polymer concentrations; (b) shrinkage and porosity of aerogels prepared with different crosslinkers at different polymer concentrations; (c) porosity of aerogels prepared with different crosslinkers and diamines at 10% polymer concentrations; (d) shrinkage of aerogels prepared with different crosslinkers and diamines at 10% polymer concentrations.

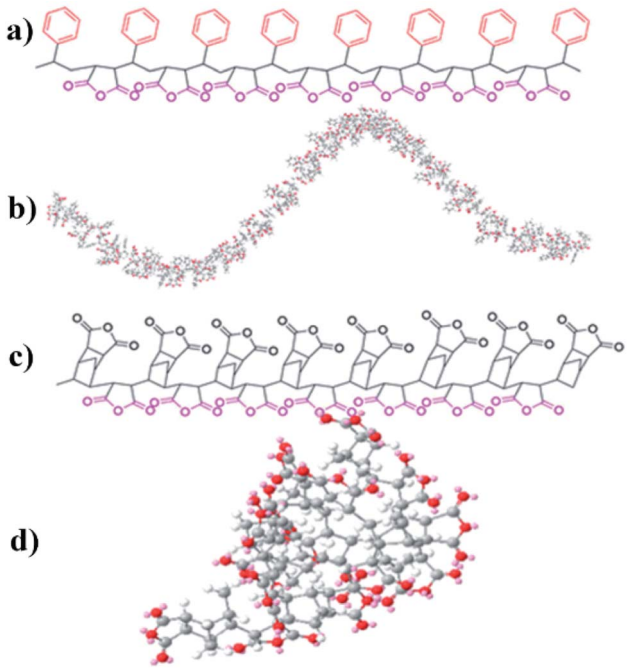

Fig. 6 (a) The structure of PSMA; (b) three-dimensional renderings of PSMA using MM2; (c) the structure of PMN; (d) three-dimensional renderings of PMN using MM2.

(Fig. 7a), indicating that the aerogels consist predominately of three-dimensional continuous meso-macro-pores. The aerogels cross-linked with PSMA show a higher specific surface area than the aerogels cross-linked with PMN (Fig. 7a). The maximum specific surface area is up to 456 m^2 g^{-1}. The specific surface area is close to those of aerogels cross-linked with TAB,[2] OAPS,[22] BTC.[28] The pore size distribution of aerogels is mainly concentrated in the range of 30–80 nm according to curves of relative pore volume *vs.* pore diameter of aerogels (Fig. 7b). The cross-linking agent influences the pore size distribution of aerogels to a certain extent. The PMN cross-linked aerogels exhibit a slightly larger pore volume and surface area according to Fig. 7c and d. It is probably attributed to the fact that PMN cross-linked aerogels exhibit less shrinkage due to molecular rigidity. Similarly, the aerogel with ODA as diamine in the backbone shows a smaller pore size average.[2]

The mechanical properties of the PI aerogels

All aerogels formulations in the study were compressed. Young's modulus of the aerogel is measured at the initial slope of the stress–strain curve, some of which are shown in Fig. 8b. Similar to aerogels cross-linked with OAPS,[22] TAB,[2] and BTC,[28] the aerogels with PMN and PSMA exhibit a linear elastic region up of 0.04 to 0.2 strain. The modulus is in the region of 1–22 MPa. And the aerogels with PMN shows a higher modulus (Fig. 8c). The maximum modulus is 21.3 MPa. As expected, the

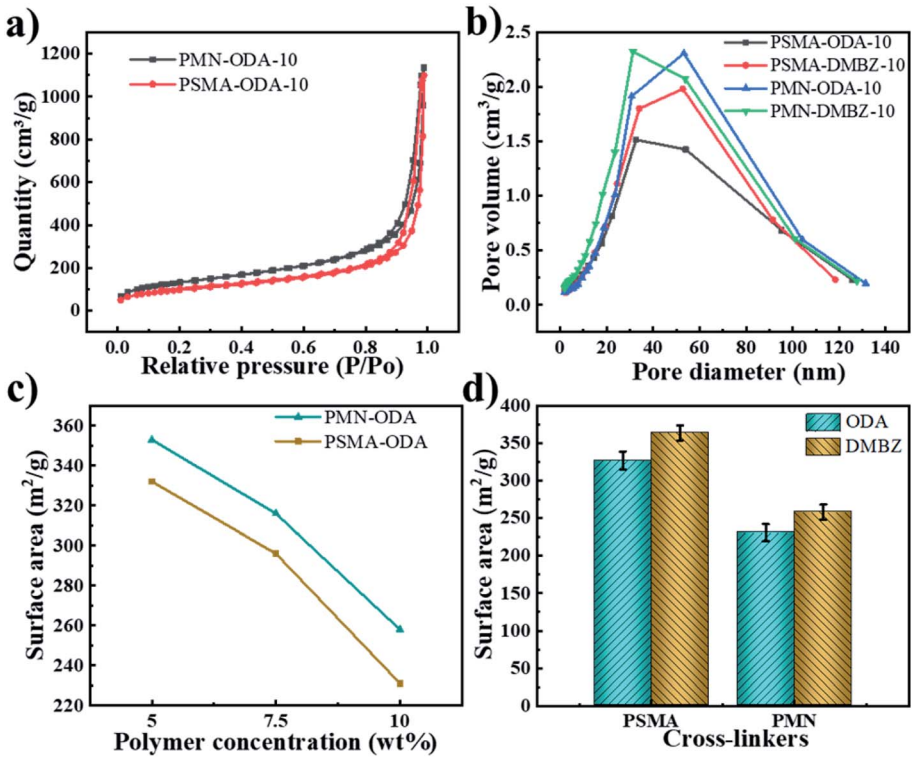

Fig. 7 (a) N_2 adsorption–desorption isotherms curves of PMN-ODA-10 and PSMA-ODA-10; (b) curves of relative pore volume *vs.* pore diameter of aerogels prepared with different crosslinkers and diamines at 10% polymer concentration; (c) surface area of aerogels prepared with different crosslinkers and the same diamines at different polymer concentration; (d) surface area of aerogels prepared with different crosslinkers and diamines at 10% polymer concentration.

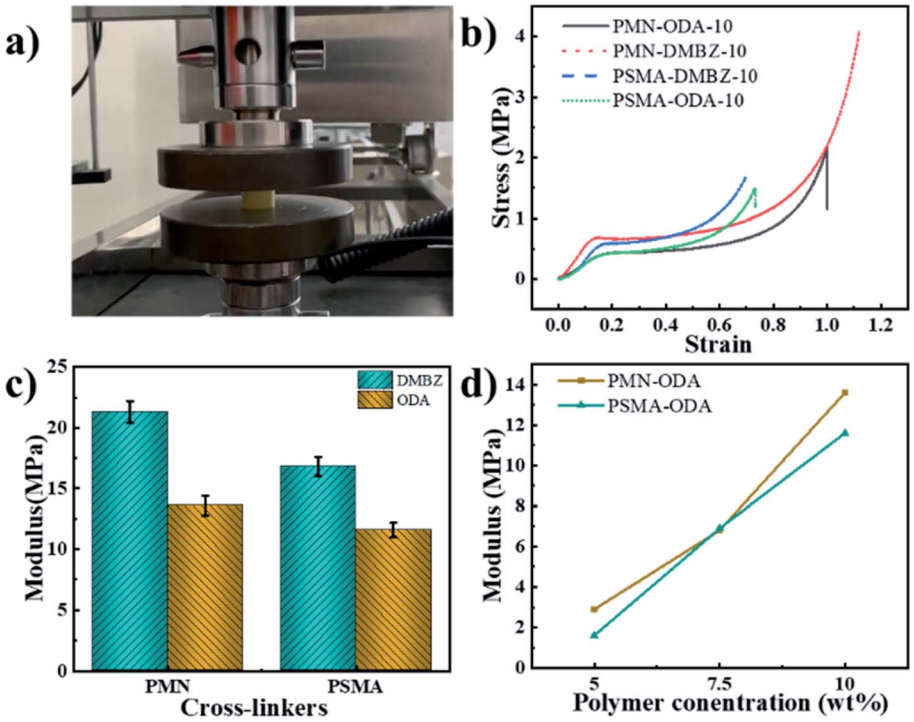

Fig. 8 (a) Images of the compressed aerogel; (b) stress–strain curves from compression of PMN-ODA-10, PMN-DMBZ-10, PSMA-DMBZ-10, and PSMA-ODA-10; (c) modulus of aerogels prepared with different cross-linkers and diamines at 10% polymer concentration; (d) modulus of aerogels prepared with different crosslinkers and the same diamines at different polymer concentration.

modulus of the aerogel gradually increases with increasing polymer concentration according to Fig. 8d. It is noticed that aerogel cross-linked with PMN exhibits both high porosity and modulus. It's possible that because PMN has both anhydrides on the polymer chain unit making the cross-linked PI show higher porosity and mechanical strength. Unfortunately, the compressive strength of the aerogel is lower than the aerogels cross-linked with OAPS,[22] TAB,[2] and BTC.[28] We speculate that this might be due to the aliphatic main chain of polymers. Which exhibit lower mechanical strength than aromatic polymers due to aggregation cross-linkers molecular.

The thermal stability of the PI aerogels

Fig. 9 illustrates the TGA curves of aerogels. The aerogels using two different cross-linkers have a similar initial decomposition temperature of 300 °C (Fig. 9a), which is higher than the initial decomposition temperature of the BTC-crosslinked aerogels.[2,22,28] The onset of thermal decomposition of aerogels with DMBZ is lower due to the presence of methyl groups. It is similar to aerogels with TAB and OAPS as cross-linkers.[2,22] The polymer concentration is independent of the thermal decomposition (Fig. 9b), as polymer concentration does not change the chemical structure of the aerogels.

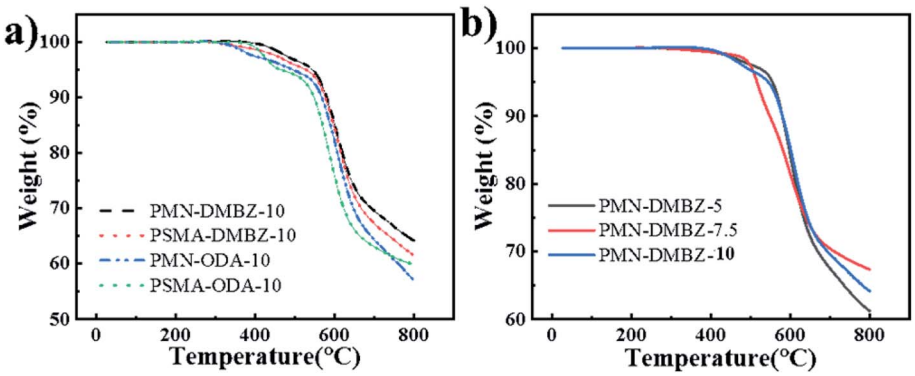

Fig. 9 (a) TGA curves of PMN-DMBZ-10, PSMA-DMBZ-10, PMN-ODA-10, and PSMA-ODA-10 aerogels; (b) TGA curves of PMN-DMBZ-5, PMN-DMBZ-7.5, PMN-DMBZ-10 aerogels.

Conclusions

Polyimide aerogels were prepared with two kinds of polymers capped polyamide oligomers, which are less costly than small-molecule cross-linkers. Compared to polyimide aerogels cross-linked with small molecule crosslinkers, the polyimide aerogels exhibit lower shrinkage and bulk density, similar specific surface area and porosity. The effect of the cross-linkers on the properties of the aerogels was discussed. Aerogels prepared with cross-linkers with different side groups and anhydride densities on cross-linker chain units have similar fibrous structures. PMN cross-linked aerogels with less shrinkage and lower density, higher porosity, and specific surface area. Aerogels cross-linked with two cross-linkers have a similar initial decomposition temperature of 300 °C. The modulus of PMN cross-linked aerogels was higher, especially when the backbone was DMBZ. In conclusion, the two cross-linkers studied can be used as low-cost alternatives to cross-link polyimide aerogels, giving them properties similar to those of other reported cross-linkers.

Conflicts of interest

There are no conflicts to declare.

Acknowledgements

This work was financially supported by National Key R&D Program of China (No. 2018YFC0807600), USTC Research Funds of the Double First-Class Initiative (No. YD2320002002), National Natural Science Foundation of China (No. 52074253), Natural Science Foundation of Anhui Province (No. 1908085ME126), and China Postdoctoral Science Foundation (No. 2020M682047).

Notes and references

1 M. A. Meador, S. Wright, A. Sandberg, B. N. Nguyen, F. W. Van Keuls, C. H. Mueller, R. Rodriguez-Solis and F. A. Miranda, *ACS Appl. Mater. Interfaces*, 2012, **4**, 6346–6353.

2 M. A. B Meador, E. J. Malow, R. Silva, S. Wright, D. Quade, S. L. Vivod, H. Guo, J. Guo and M. Cakmak, *ACS Appl. Mater. Interfaces*, 2012, **4**, 536–544.

3 (*a*) X. Li, J. Wang, Y. B. Zhao and X. T. Zhang, *ACS Appl. Mater. Interfaces*, 2018, **10**, 16901–16910; (*b*) Y. L. Pan, X. D. Cheng, T. zhou, L. L. Gong and H. P. Zhang, *Mater. Lett.*, 2018, **229**, 265–268.

4 X. Z. Guo, J. Q. Shan, W. Lei, R. H. Ding, Y. Zhang and H. Yang, *Polymers*, 2019, **11**, 375–390.

5 (*a*) A. Lamy-Mendes, R. F. Silva and L. Durães, *J. Mater. Chem. A*, 2018, **6**, 1340–1369; (*b*) Y. L. Pan, S. He, L. L. Gong, X. D. Cheng, C. C. Li, Z. Li, Z. Liu and H. P. Zhang, *Mater. Des.*, 2017, **113**, 246–253.

6 M. Wiehn, T. J. Levario, K. Staggs, N. Linneen, Y. C. Wang, R. Pfeffer, Y. S. Lin and D. R. Nielsen, *Ind. Eng. Chem. Res.*, 2013, **52**, 18379–18385.

7 X. Wang and S. C. Jana, *ACS Appl. Mater. Interfaces*, 2013, **5**, 6423–6429.

8 J. Xiao, J. Zhang, W. Lv, Y. Song and Q. Zheng, *Carbon*, 2017, **123**, 354–363.

9 J. Feng, C. Zhang, J. Feng, Y. Jiang and N. Zhao, *ACS Appl. Mater. Interfaces*, 2011, **3**, 4796–4803.

10 S. Mahadik-Khanolkar, S. Donthula, C. Sotiriou-Leventis and N. Leventis, *Chem. Mater.*, 2014, **26**, 1303–1317.

11 L. H. Zhuo, C. Ma, F. Xie, S. S. Chen and Z. Q. Lu, *Cellulose*, 2020, **27**, 7677–7689.

12 Y. Wang, Z. H. Zhou, C. G. Zhou, W. J. Sun, J. F. Gao, K. Dai, D. X. Yan and Z. M. Li, *ACS Appl. Mater. Interfaces*, 2020, **12**, 8704–8712.

13 X. H. Zhang, X. X. Ni, C. X. Li, B. You and G. Sun, *J. Mater. Chem. A*, 2020, **8**, 9701–9712.

14 Y. X. Wang, T. J. He, Z. Cheng, M. Y. Liu, J. Q. Ji, X. H. Chang, Q. Xu, Y. Liu, X. Y. Liu and J. Q. Qin, *Compos. Sci. Technol.*, 2020, **195**, 108204–108212.

15 L. L. Xu, L. H. Xiao, P. Jia, K. Goossens, P. Liu, H. Li, C. G. Cheng, Y. Huang, C. W. Bielawski and J. X. Geng, *ACS Appl. Mater. Interfaces*, 2017, **9**, 26392–26399.

16 R. P. Viggiano, J. C. Williams, D. A. Schiraldi and M. A. Meador, *ACS Appl. Mater. Interfaces*, 2017, **9**, 8287–8296.

17 B. N. Nguyen, M. A. B. Meador, D. Scheiman and L. McCorkle, *ACS Appl. Mater. Interfaces*, 2017, **9**, 27313–27321.

18 B. N. Nguyen, E. Cudjoe, A. Douglas, D. Scheiman, L. McCorkle, M. A. B. Meador and S. J. Rowan, *Macromolecules*, 2016, **49**, 1692–1703.

19 C. Chidambareswarapattar, Z. Larimore, C. Sotiriou-Leventis, J. T. Mang and N. Leventis, *J. Mater. Chem.*, 2010, **20**, 9666–9678.

20 N. Leventis, C. Sotiriou-Leventis, D. P. Mohite, Z. J. Larimore, J. T. Mang, G. Churu and H. b. Lu, *Chem. Mater.*, 2011, **23**, 2250–2261.

21 H. Q. Guo, M. A. Meador, L. McCorkle, D. J. Quade, J. Guo, B. Hamilton, M. Cakmak and G. Sprowl, *ACS Appl. Mater. Interfaces*, 2011, **3**, 546–552.

22 H. Q. Guo, M. A. Meador, L. McCorkle, D. J. Quade, J. Guo, B. Hamilton and M. Cakmak, *ACS Appl. Mater. Interfaces*, 2012, **4**, 5422–5429.

23 M. A. Meador, E. McMillon, A. Sandberg, E. Barrios, N. G. Wilmoth, C. H. Mueller and F. A. Miranda, *ACS Appl. Mater. Interfaces*, 2014, **6**, 6062–6068.

24 J. Feng, X. Wang, Y. Jiang, D. Du and J. Feng, *ACS Appl. Mater. Interfaces*, 2016, **8**, 12992–12996.

25 H. Q. Guo, M. A. B. Meador, L. S. McCorkle, D. A. Scheiman, J. D. McCrone and B. Wilkewitz, *RSC Adv.*, 2016, **6**, 26055–26065.

26 Z. Zhang, X. D. Wang, G. Q. Zu, L. Liu, X. X. Zhang, S. Xi, H. Y. Zhao and J. Shen, *J. Supercrit. Fluids*, 2020, **160**, 104811–104818.

27 M. Chao, Y. M. Li, G. L. Wu, Z. J. Zhou and L. K. Yan, *Int. J. Polym. Sci.*, 2019, **2019**, 1–12.

28 M. A. Meador, C. R. Aleman, K. Hanson, N. Ramirez, S. L. Vivod, N. Wilmoth and L. McCorkle, *ACS Appl. Mater. Interfaces*, 2015, **7**, 1240–1249.
29 X. F. Zhang, X. Cui, C. H. Lu, H. Li, Q. Zhang, C. G. He and Y. K. Yang, *Chem. Eng. J.*, 2020, **401**, 126031–126041.
30 S. Lei, X. Cui, X. F. Liu, X. F. Zhang, X. Y. Han and Y. K. Yang, *Chem. Commun.*, 2020, **56**, 1429–1432.
31 X. Cui, L. K. Gao, S. Lei, S. Liang, J. Zhang, C. D. Sewell, W. D. Xue, Q. Liu, Z. Q. Lin and Y. K. Yang, *Adv. Funct. Mater.*, 2020, **31**, 2009197.